esa
headquarters

8-1o rue Mario Nikis
75738 Cedex 15 Paris
France
www.esa.int

DOCUMENT

ASTEROID IMPACT MISSION: DIDYMOS REFERENCE MODEL

Issue 3
Revision 1
Date of Issue 20/11/2015
Status Released
Document Type AD

European Space Agency
Agence spatiale européenne

Table of contents:

1. INTRODUCTION

1.1. Scope

This document shall serve as the reference model of the asteroid 65803 Didymos 1996 GT and the radiation environment encountered by the AIM spacecraft. It shall be used by the Contractor throughout the AIM phase-A/B1 study tasks.

Any missing or conflicting information deemed necessary for the AIM spacecraft design shall be reported to the Agency, which will maintain this model and make updates available as necessary in the context of the AIM Phase A/B1 work.

A revised shape model of Didymos' primary is to be expected at phase-B1 kick-off, accounting for both radar and the most recent lightcurve data.

2. REFERENCES

[1] Minor Planet Center: last update by Pan-STARRS 1

[2] PDS, radar (Lance Benner) and lightcurve (Petr Pravec) observations.

[4] Pravec, P., et al., 2006, Photometric survey of binary near-Earth asteroids, Icarus, 181:63-93.

[5] Fang, J., and J.-L. Margot, 2012, Near-Earth binaries and triples: Origin and evolution of spin-orbital properties, Astron. J., 143:24.

[6] Scheirich, P., and P. Pravec, 2009, Modeling of lightcurves of binary asteroids, Icarus, 200:531-547.

[7] JPL Small-Body Database Browser: http://ssd.jpl.nasa.gov/sbdb.cgi

[8] Asteroid Lightcurve DataBase, rev. 2014-Mar-01

[9] AIM Advisory Team Final Report: https://www.oca.eu/michel/AIMReport_Final.pdf

[10] Pravec et al. 2012, Absolute magnitudes of asteroids and a revision of asteroid albedo estimates from WISE thermal observations, Icarus 221: 365-387.

[11] Hideaki Miyamoto, et al., Regolith Migration and Sorting on Asteroid Itokawa, Science 316, 1011 (2007)

[12] Michikami T. et al., 2008 Size-frequency statistics of boulders on global surface of asteroid 25143, Itokawa, Earth Planets Space, 60, 13–20, 2008

[13] Maruyama, S. et al., Evidence for Global-Scale Inverse Grading of Regolith Materials on Asteroid Itokawa, 41st Lunar and Planetary Science Conference (2010) #1577

[14] Michikami, T., A. M. Nakamura, et al. (2010). "The shape distribution of boulders on Asteroid 25143 Itokawa: Comparison with fragments from impact experiments." Icarus 207(1): 277-284.

[15] Mazrouei et al., Icarus 229 (2014) 181–189

[16] Kitazato et al. (2004). Photometric Behaviour Dependent on Solar Phase Angle and Physical Characteristics of Binary Near-Earth-Asteroid (65803) 1996 GT. 35th Lunar and Planetary Science Conference, March 15-19, 2004, League City, Texas, abstract no.1623.

[17] ECSS-E-ST-10-04C, "System Engineering: Space Environment Standard", November 2008.

[18] Seltzer S., "SHIELDOSE: A Computer Code For Space Shielding Radiation Dose Calculations," NBS Technical Note 1116, National Bureau of Standards, May 1980.

[19] https://www.spenvis.oma.be/

[20] I. Jun et al. "Proton Nonionizing Energy Loss (NIEL) for Device Applications," IEEE Trans. Nucl. Sci. Vol 50, No 6, Dec 2003.

[21] A.J. Tylka et al. "CREME96: A Revision of the Cosmic Ray Effects on Micro-Electronics Code", IEEE Trans. Nucl. Sci. NS-44, 2150-2160 (1997).

3. TERMINOLOGY & ACRONYMS

+/-	Refers to the uncertainty of the reported value without giving the nature of the uncertainty.
[#]	Reference (as detailed in section 2).
P	period
a	semi-major axis
e	eccentricity
i	inclination
ρ	bulk density
D	Mean (volume-equivalent) diameter, i.e., the diameter of a sphere with the same volume
MPC	Minor Planet Center
Subscripts P, S, orb	Primary, Secondary, Orbit of secondary around primary
r_{PS}	Position vector of S with respect to P
a_x, b_x, c_x	long, intermediate, and short axis of the ellipsoid representing body X
TI	Thermal inertia (in SI units)
SED	Spectral energy distribution

If not stated otherwise, error bars represent 1sigma bounds.

4. MAIN DYNAMICAL AND OBSERVATIONAL VALUES

The only dynamical parameters measured directly through observations are the orbital period of the secondary around the primary, their orbital separation, the rotation period of the primary and the size ratio of secondary to primary. They are indicated in bold in the following table. All other quantities (e.g. system's mass etc.) are derived from these measured parameters. A shape model (and a volume) of the primary is also derived from radar observations combined with optical lightcurve data, from which a bulk density estimate is inferred.

The following tables give the resulting parameters (directly measured and derived) for the Didymos system. All errors are 1-sigma unless stated otherwise, and all extra-digits are given for consistency with the directly measured parameters.

Parameter	Value	Reference / comments
Official minor planet number of primary	65803	[1]
Official name of primary	Didymos	[1]
Provisional designation of primary	1996 GT	[1]
Dynamical type	Apollo	[1]
Method of discovery of companion	photometric lightcurve	[1]
Last update in MPC database	21 May 2015	[1]
Diameter of Primary D_P[1]	0.775 km +/- 10%	[2]
Diameter of Secondary D_S	0.163 km +/- 0.018 km	[see D_S/D_P below]
Bulk density of the primary ρ_P[2]	2146 kg m^{-3} +/- 30%	[from D_P. M_{tot}]
Secondary (shape) elongation a_s/b_s	1.3 +/- 0.2	See section 6 for details on shape

[1] The values of the primary and secondary diameters, as well as the optical and radar albedos, correspond to the baseline pole solution indicated in section 5.

[2] The bulk density of the secondary is not known. However, based on the known bulk density range for S-type objects (about 2000 to 2700 kg m^{-3}, we assume a value of 2146 kg m^{-3} for the secondary. Even if the secondary may be a rubble pile, it should be relatively compact because indications hint to a tidally locked configuration along its major axis — this implies internal dissipation that may have helped drive the system to a lower energy state commensurate with compaction. If true, then the minimum density of the secondary should be close (but no necessarily identical) to the primary density, hence the assumed value of 2146 kg m^{-3}.

and b_s/c_s (assumed)[3]	>1 (assumed 1.2)	model
Distance between the centre of primary and secondary a_{orb}	**1.18 km +0.04/-0.02 km**	[5]
Total mass of system	5.278e11 kg +/-0.54e11 kg[4]	[5]
Geometric Albedo	0.15 +/- 0.04	[from D_P, D_S, H]
Rotation period of the primary	**2.2600 h +/-0.0001 h**	[4]
Radar albedo	0.27 +/-25%	[2]
Heliocentric eccentricity e	e = 0.383752501 +/- 7.7e-9	[7]
Heliocentric semimajor axis a	1.6444327821 +/- 9.8e-9 AU	[7]
Heliocentric inclination to the ecliptic i[5]	3.4076499° +/- 2.4e-6°	[7]
Mean absolute magnitude (whole system) H	18.16 +/- 0.04	[10]

The primary's mass estimate and its volume for the current (preliminary) radar shape model lead to a primary bulk density of 2146 kg m^{-3} with a substantial (conservative) uncertainty of about 30%. The Contractor shall assume a **bulk density of 2146 kg m^{-3} for both the primary and the secondary.** This assumption may change when an updated shape model (under construction) becomes available, combining the data obtained from both radar and lightcurve observations.

Under the assumption that the two components have the same bulk density, the mass of the secondary with respect to that of the primary depends on the diameter ratio:

$$M_S / M_P = V_S/V_P = (D_S / D_P)^3 = (0.21 +/- 0.01)^3 = 0.0093 +/- 0.0013$$

[3] a_s/b_s from Pravec et al. in preparation. Note that we do not have any direct observation of the Didymoon's shape. This value is thus assumed from the average value observed for other binary systems. An ellipsoidal shape is assumed with $a_s \geq b_s \geq c_s$. The assumed b_s/c_s is based on the observations of similar systems. The rotation state is not constrained by observations and may be unstable (tumbling) for a_s/b_s~1.4. a_s is oriented in the x axis of the corotating frame, i.e. in the direction connecting the CoMs of the two bodies.

[4] Derived from the observation of period, and inferred semi-major axis; Error bars computed by Lance Benner.

[5] The orbital elements are given at epoch 2457000.5 (2014-Dec-09.0), reference: JPL 120 (heliocentric ecliptic J2000); 2015-Jun-04 18:20:59 .

5. BINARY ORBIT SOLUTIONS

Of the two pole solutions originally reported in [6], an observation campaign performed by the Discovery Channel Telescope on 2015-04-13 favours the **retrograde orbit solution 2**, and it constrains this solution further.

Synchronous rotation of secondary is compatible with existing observations. This would imply the secondary rotational period P_S is the same as the secondary orbital period P_{orb}.

Binary Orbit Solution 2	Baseline solution	
Pole solution 2	λ=310°, β=-84°	[6, updated] (Ecliptic coordinates)
Obliquity to the heliocentric orbit	171° +/- 9°	(3σ error bars)
Diameter ratio D_S/D_P	**0.21 +/- 0.01**	[6]
Secondary orbital period P_{orb}	**11.920h +0.004/-0.006**	[6]
Secondary orbital eccentricity e	0.03 (upper limit)	[6]
Secondary orbital inclination i_{orb} (assumed)	0°	Primary equatorial coordinates
Obliquity of the primary principal axis with respect to the mutual orbital plane (assumed)	0°	
Obliquity of the secondary principal axis with respect to the mutual orbital plane (assumed)	0°	

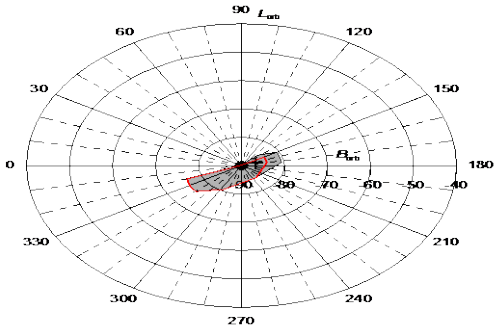

Figure 1 *The allowed (3-σ) area of the retrograde pole of the mutual orbit in ecliptic coordinates. The grey area was derived from the 2003 + 2015 photometric observations. The red curve is an outline of the area that was further constrained with the modeling refined using the preliminary primary shape model. The cross is the south pole of Didymos' heliocentric orbit.*

6. RADAR SHAPE MODEL

A preliminary shape model of the Didymos primary based on the past radar observations in combination with new lightcurve data is shown below in Fig. 2. This model is not the very final one but already close to it.

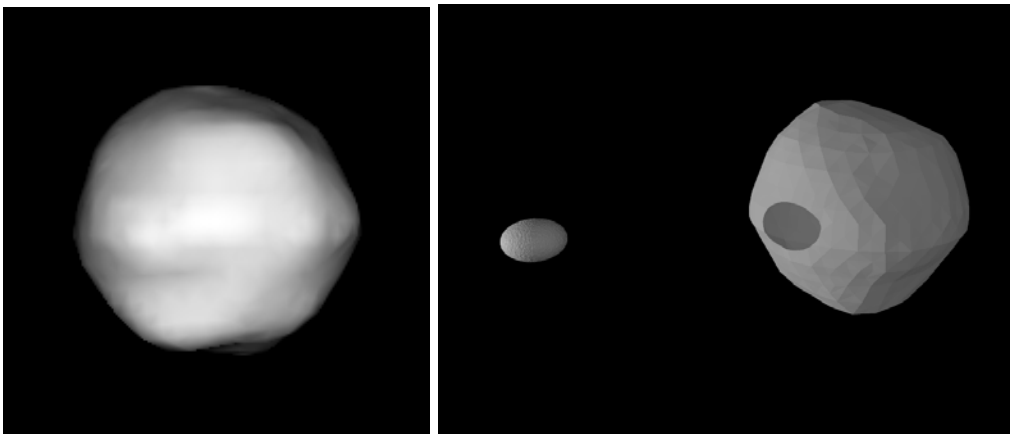

Figure 2: *Left: preliminary shape model of the primary (principal axis view) for the radar pole solution close to the baseline pole solution. The secondary (not imaged) estimated to be more elongated from other data (courtesy of L. Benner and S. Naidu). Right: Didymain and Didymoon at scale (courtesy of S.R. Schwartz).*

Radar data cannot provide a model of the secondary since the SNR is too weak, echoes are not sufficiently resolved and the rotation coverage is limited. For modelling purposes, the shape of the secondary is *assumed* to be a triaxial ellipsoid with the

axes ratio ranges given in section 4. The long axis a_s is assumed to be oriented, on average, in the x axis of the corotating frame, i.e. in the direction that connects the CoM of Didymain and Didymoon, the c_s axis is identified with the assumed secondary spin direction. The b_s axis is in the mutual orbit plane since the obliquity of the secondary is assumed to be 0°. The numerical value of the axes follows from the condition of volume equivalence of the ellipsoid 4/3*pi*a*b*c to 4/3*pi*(0.163)^3/8 [km], thus a_s=103 m. The nominal values of the minor axes are b_s=79 m, c_s=66 m. Note that these values are being checked within a study of the system's stability.

7. DIDYMOON'S ESCAPE VELOCITY

Any requirement based on the escape velocity should consider an escape velocity v_{esc} calculated considering 3-body effects (i.e. opening/closure of L1 and L2 necks as a function of the lander kinetic energy). Values for v_{esc} depend on whether the L1 or L2 neck opening is considered. The effect of physical parameters dispersion on these values is to be assessed.

For a classic circular restricted 3-body problem, in the corotating frame:

- L1 is at [1005.476; 0; 0] m
- L2 is at [1348.267; 0; 0] m

Without modification of the orbital parameters, but accounting for Didymoon's shape for the computation of the Lagrange points, in the co-rotating frame:

- L1 is at [999.309; 0; 0] m
- L2 is at [1354.372; 0; 0] m

The escape speeds are computed over the surface of Didymoon. The L1 (resp. L2) escape speed of a given point is defined as the smallest speed that opens the zero-velocity surfaces at L1 (resp. L2). The L1 (resp. L2) escape speed for a body is defined as the smallest L1 (resp. L2) escape speed across its surface.

Because L1 always opens before L2, the most conservative escape speed that can be taken is to consider the L1 escape speed. However, one should note that many impacting trajectories are not favourably oriented after bounce to reach L1. Thus this criterion is conservative.

The L1 escape speed for Didymoon with the current model is 4.146 cm/s.
The L2 escape speed for Didymoon with the current model is 4.612 cm/s.

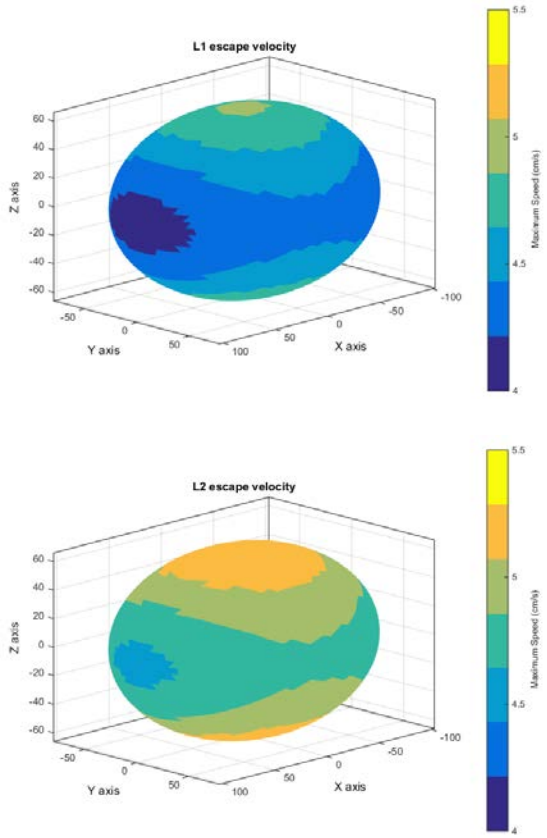

Figure 3: *Escape speeds at L1 (top) and L2 (bottom) over the surface of Didymoon (courtesy of Simon Tardivel).*

8. SURFACE (ROCK) MODEL OF DIDYMOON

The cumulative number of rocks with diameter greater or equal to a given diameter D (in m), per square meter, is given by N(D).

The differential size frequency distribution (SFD) of surface rocks is assumed to follow a power law described by $dN = KD^q dD$ where dN *is* the number of boulders per unit area in the diameter range between D (typically, the long diameter of an ellipse fitted to the image) and $D+dD$, and where K and q *(-4.5<q<-3)* are constants of the power-law. The cumulative distribution N_c (N>D) is the integral of the differential distribution, or

$$N_c(N>D) = \int dN = \int KD^q\, dD = \frac{K}{q+1} D^{q+1} = cD^p$$

$$p = q+1, c = -K/(q+1) = -K/p$$

Note that the measurement error of any N in a bin is given by $\sqrt{N}$ (Poisson statistics). However, such a power law holds only over limited ranges of D and leads to unphysical results for D tending to 0 and for very large D.

Nothing is known observationally about the rock size distribution on Didymoon. We assume the cumulative size distribution as given by a power law with an exponent between -2 and -3.5 (as observed for many bodies and consistent with theoretical expectations) and define two extreme cases, "smooth" vs. "rocky". These were derived from scaling the rock size distribution on Itokawa [11-14] between 0.2 m and 25 m and scaled to unit area by Itokawa's surface (0.4011 km², [15]).

Cutoff diameters: Pebbles, cobbles, and boulders represent objects whose sizes range in 4mm-6.4cm, in 6.4c m-2.6 m, and in >2.6m, respectively; gravel includes all of them. Pebbles are not regarded as rocks but rather as part of the regolith. Very large boulders can be modeled as part of the shape model.

8.1. Model parameters

Lower cutoff diameter: 6.4 cm
Upper cutoff diameter: 5 m (TBC)
Exponent a= -2.5+/-0.5

Scaling factors (all TBC):

	"Smooth"	"Nominal"	"Rocky"
c (1/m²)	0.012	0.12 [11]	0.24
K (1/m²)	0.030	0.30 [11]	0.60

Where "Smooth" is Itokawa/10, "rocky" is Itokawa x2 and close to saturation at the lower cutoff). The nominal surface[6] of Didymoon is about 85660 m² (+/- 22%).

9. THEORETICAL THERMAL MODEL

The thermal properties of the surface (e.g. thermal inertia) will not be known before AIM rendezvous with Didymos. A modelled temperature map of the far side of Didymoon for nominal and extreme (high and low) possible thermal properties have been obtained assuming a spherical shape for the body.

9.1. Assumed properties for detailed thermal modelling of Didymoon

Thermal inertia of the surface: 50 J m^{-2} K^{-1} $s^{-1/2}$ (minimum)
1000 J m^{-2} K^{-1} $s^{-1/2}$ (maximum)
Bolometric Bond albedo of the primary[7]: A = 0.07 ± 0.02

[6] Surface of nominal tri-axial ellipsoid approximated with the Knud-Thomsen formula.
[7] Based on that of the primary (with phase integral 0.4268 from G = 0.20 +/- 0.02 measured by [16] and assumed p_V = 0.15 similar to primary's albedo).

Emissivity: 0.9

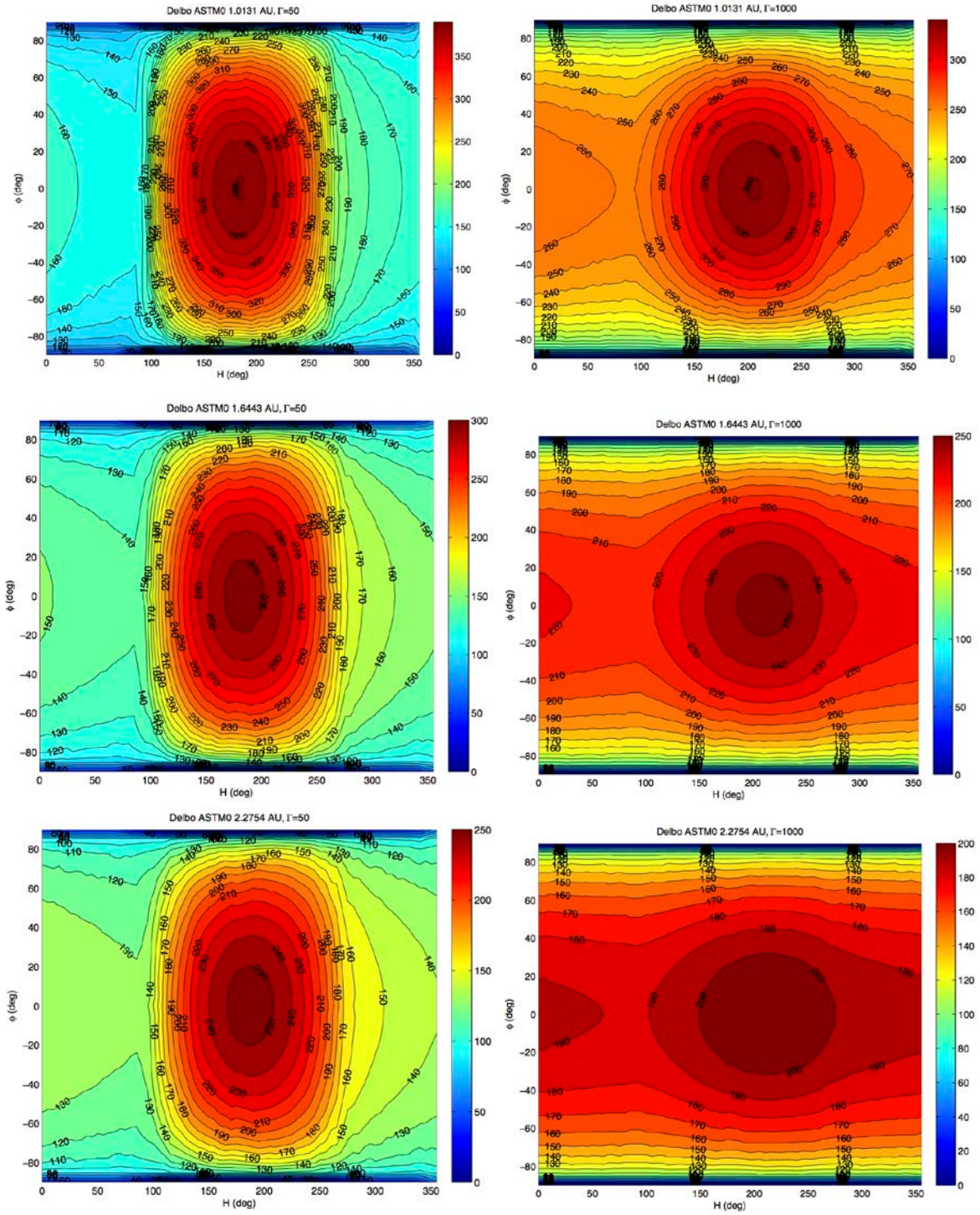

Figure 4: *Temperature maps of the far side of Didymoon for nominal and extreme (high and low, from left to right) possible thermal properties assuming a spherical shape of the body and for closer and larger*

distances to the Sun (from top to bottom). Courtesy of M. Delbo.

10. RADIATION ENVIRONMENT

10.1.The underlying environment model

This section contains a preliminary specification for the environment to be encountered by the planned Asteroid Impact Mission (AIM). See Appendix A for a list of all applicable assumptions to the analysis. Based on the present ECSS standard the solar energetic particle model applied is the PSYCHIC model [17], which is run with a confidence of 95% due to uncertainties in the present mission parameters. Figure 3 and Table 1 in Appendix B provide the solar proton fluence spectra for the different mission phases.

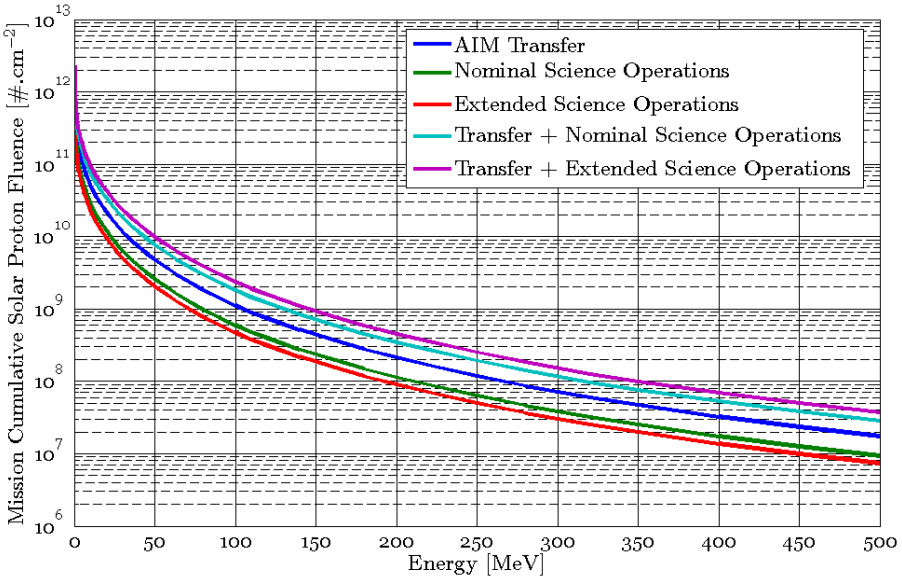

Figure 3 *Solar proton spectrum as a function of integral energies for the various mission phases for AIM based on a 2020 launch.*

10.2. Total Ionizing Dose

The total ionizing dose (TID) environment is represented by the dose-depth curve. This may provide dose as a function of shield thickness in planar geometry or as a function of spherical shielding about a point. The planar model is appropriate for surface materials or for locations near to a planar surface. In general, electronic components are not in such locations and a spherical model is recommended for general specification.
The SHIELDOSE model shall be used [18] for ionizing dose. This method uses a pre-computed data set of doses from electrons, electron-induced Bremsstrahlung and protons, as derived from Monte-Carlo analysis. The doses are provided as functions of material shielding thickness. The reference geometrical configuration for this dose-depth curve shall be a solid aluminium sphere. The TID calculations are shown in Figure 4 and Table 2 in Appendix B.

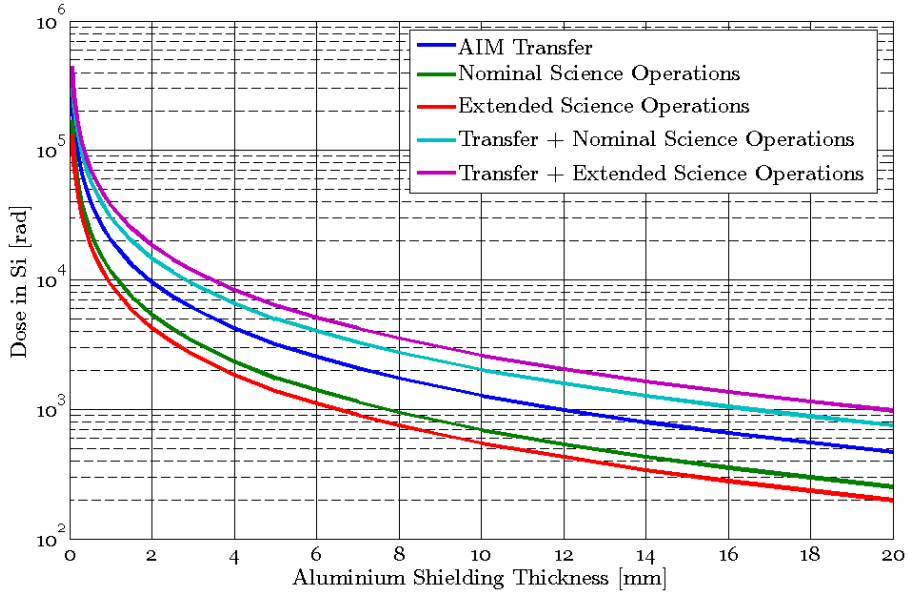

Figure 4 *Total ionizing dose in silicon as a function of spherical shielding thickness for the various mission phases for AIM based on a 2020 launch.*

10.3. Non-ionizing dose

The non-ionising dose (NID) is calculated by folding the shielded fluence as a function of energy with the non-ionizing energy loss (NIEL) damage curve (NIEL as a function of energy). In order to obtain damage equivalent fluences at a single energy for the testing of components the NIEL damage curve is normalised to the given energy and then the shielded fluences can be reduced to a single value for each shielding thickness. The NIEL damage curve used for this analysis is that labelled 'Messenger Si' on the Spenvis system [19] following result published by Jun et al. [20] and is shown in Figure 5 along with the normalisation to 10 MeV. The equivalent fluence for 10 MeV protons is provided to compare with NID dose limits is given in Figure 6 and Table 3 (Appendix B). The NIEL data are given in Figure 7 and Table 4 (Appendix B).

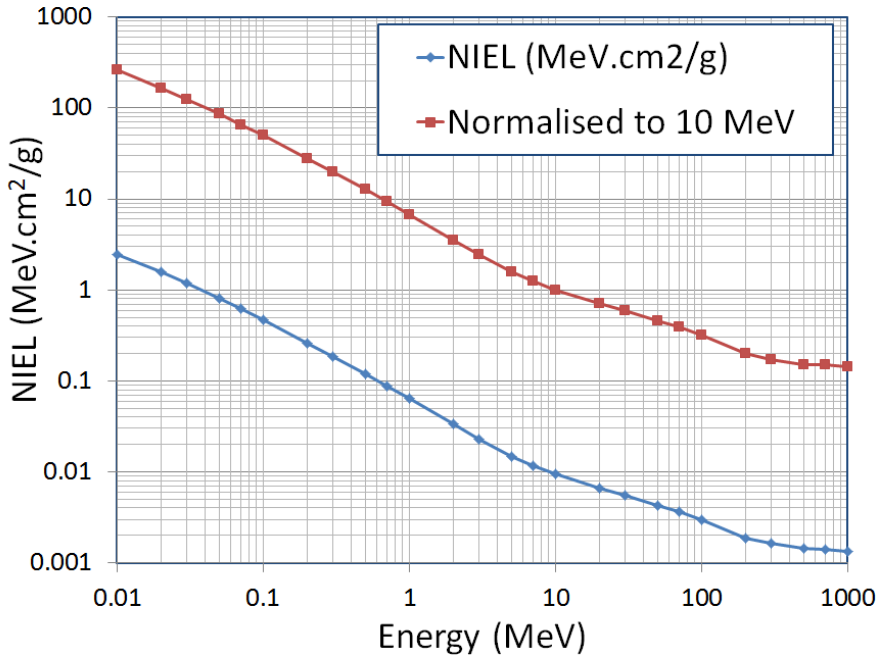

Figure 5 *NIEL damage curve in silicon and normalisation to 10 MeV protons.*

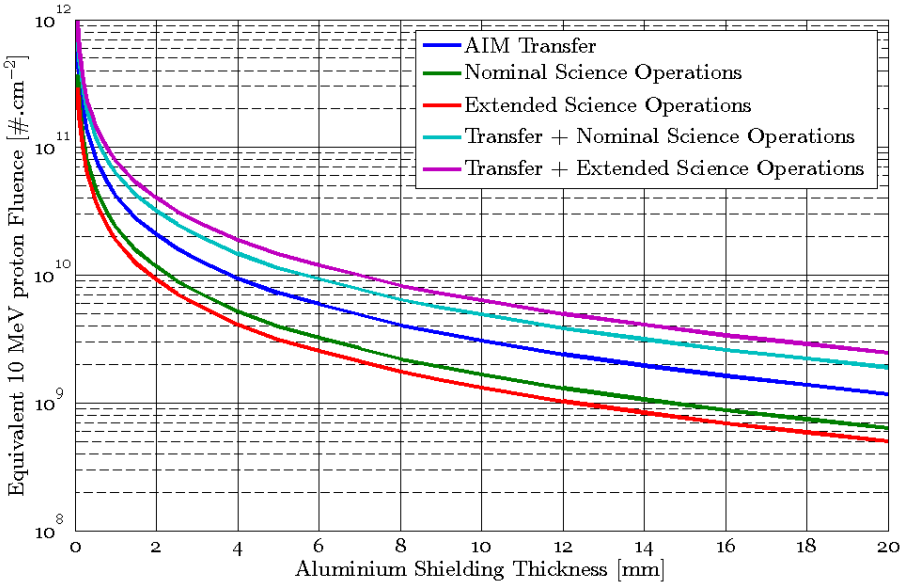

Figure 6 *Non-ionising energy loss equivalent 10 MeV proton fluence as a function of shielding thickness for the various phases of the mission based on 2020 launch of AIM.*

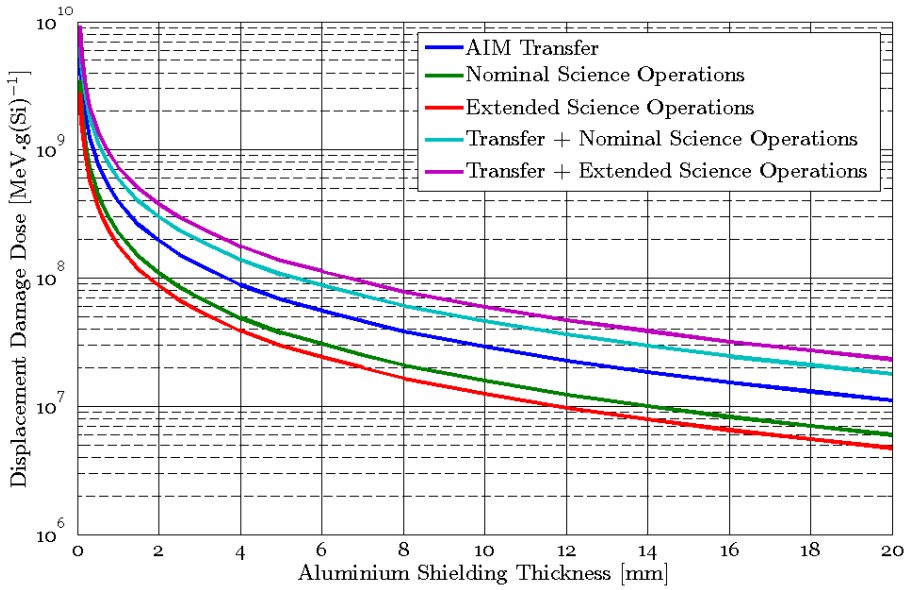

Figure 7 *Non-Ionising Energy Loss as a function of shielding thickness for the various phases of the mission based on 2020 launch of AIM.*

10.4. Single Event Effects Environment

Single Event Effects (SEEs) are a function of the density of energy deposition by ionizing radiation as this is governs the probability of such events. This energy deposition is characterised by the particle linear energy transfer (LET), which gives the amount of dose being deposited per unit shielding thickness. The CREME96 [21] spectra for GCR background, worst week and worst 5-minutes covering protons and heavy ions are given in Table 5 in Appendix B and shown in Figure 8. In order to derive the upset rate for an electronic device the geometry and critical charge to cause upsets are needed. The precursor analysis herein is performed assuming a nominal shielding thickness of 1 g.cm^{-2}.

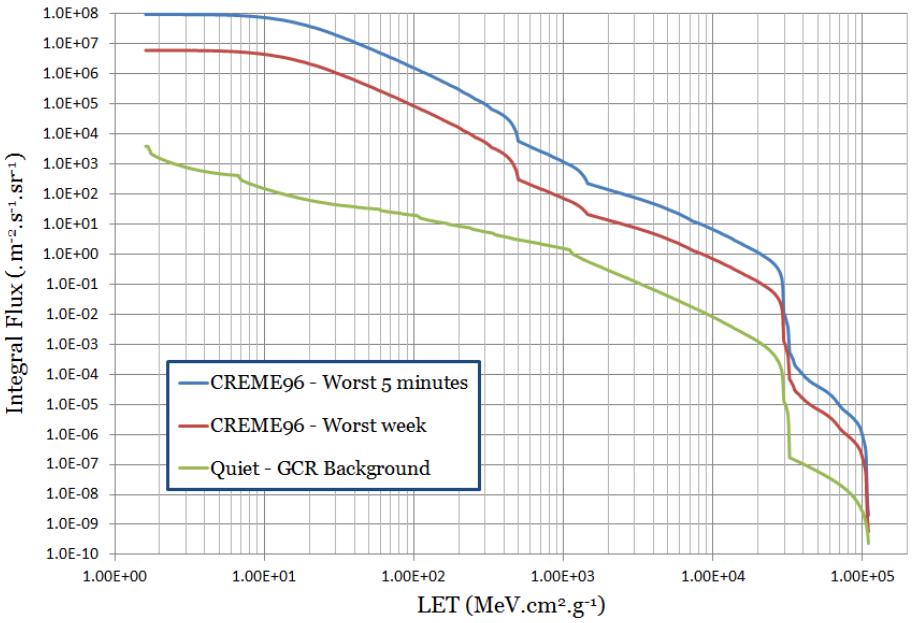

Figure 8 *LET spectra for CREME96 worst 5 minutes, worst week and quiet (GCR-only) as a function of LET for calcualtion of SEE/SEU rates.*

11. ADDITIONAL NOTES

11.1. Spectral properties

Regarding its spectral properties (ref. Figure 9), Didymos is now classified as an S-type (DeLeon et al. 2010), even if it was originally classified as an Xk-type (Binzel et al. 2004) due to limited wavelength coverage. The spectrum looks similar to that of Itokawa, which has a composition close to LL chondrites based on the analysis of the returned samples. The radar albedo is consistent with silicates and inconsistent with pure metal.

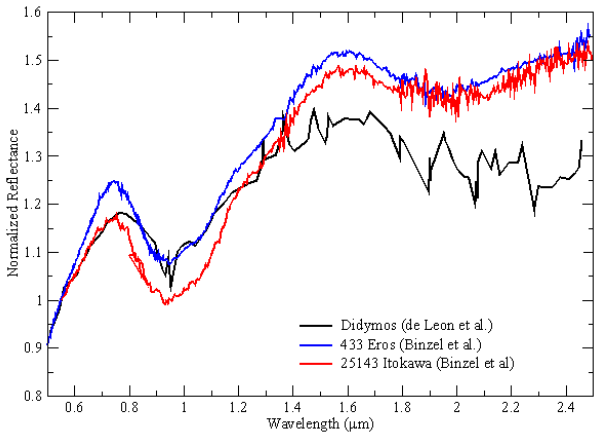

Figure 9 *Spectrum of Didymos (black) compared with that of Eros (blue) and Itokawa (red).* Taken from http://www.iac.es/proyecto/pcssolar/pages/en/data/nemcass.php.

11.2. Temperature map of Didymain

The temperature map of Didymain has been calculated (Figure 11), using the original shape model, for a thermal inertia of 100 J m^{-2} K^{-1} $s^{-1/2}$, bolometric Bond albedo of 0.1, emissivity of 0.9, and assuming the asteroid spin vector is perpendicular to the direction toward the Sun (which is not necessarily the case).

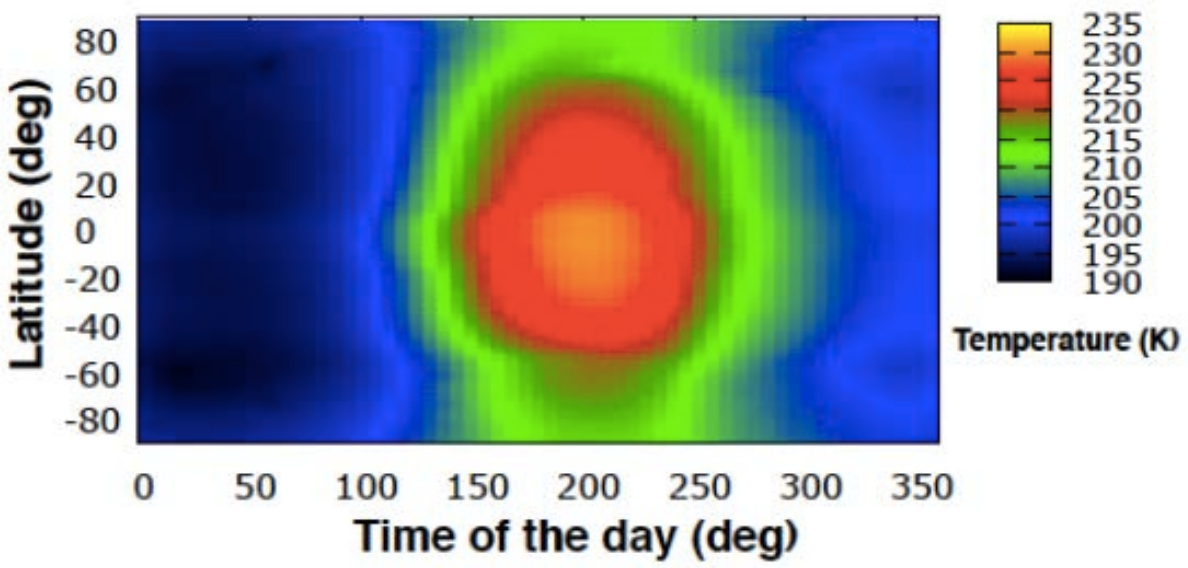

Figure 11 *Preliminary temperature distribution at the surface of the asteroid Didymos calculated at 1.664 AU from the Sun.*

Local midnight corresponds to 0 degrees. The hottest spot is not at 180 degrees (noon), but is slightly shifted because of the thermal inertia.

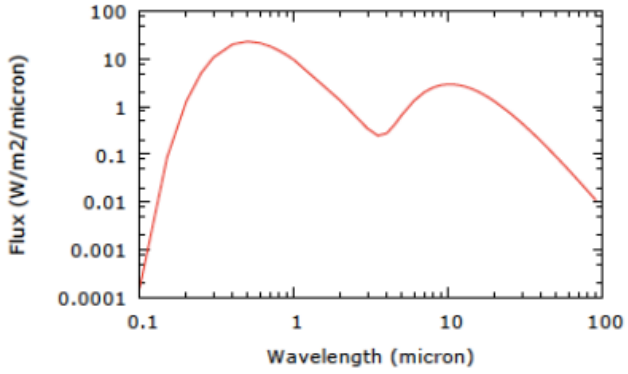

Figure 12 *Spectral energy distribution (SED) at a distance of 1 km from the asteroid.*

The total power from the asteroid and thus heating of the spacecraft is given by the integral of the SED, shown in Figure 12. This gives a flux of about 66 W/m^2.

APPENDIX A

The following assumptions have been made in the radiation analysis:

- Due to a lack of certainty on the mission parameters (namely the duration of the different mission segments) a conservative confidence level of 95% has been selected.
- Due to a lack of information about the type of solar cells to be used solar cell degradation analyses are not included.
- In the absence of the mission ephemeris it is assumed that this interplanetary mission spends very little time travelling through the Earth's radiation belts and it is therefore inherently assumed that their contribution to dose is negligible when compared to solar energetic particle fluxes.
- The local environment of the asteroid may have a significant dust/plasma effects.
- The longest mission period considered is 3 years, as such all dose analyses are done based on an assumption of the complete mission at solar maximum that being the most conservative approach.
- It is assumed that the spacecraft will spend no time closer to the Sun than 1 AU, as such, in accordance with the present ECSS standard [10], the 1 AU solar energetic particle fluxes are unscaled.

	Start Date [yyyy-mm-dd]	End Date [yyyy-mm-dd]	Duration [days]	Confidence Level [%]
Transfer (Cruise)	2020-10-17	2022-04-17	547	95
Science Operations (Nominal)	2022-04-17	2023-02-17	306	95
Science Operations (Extended)	2023-02-17	2023-10-17	242	95
Total Mission (Nominal)	2020-10-17	2023-02-17	853	95
Total Mission (Extended)	2020-10-17	2023-10-17	1095	95

Table 1 Mission parameters for each phase used in this analysis.

APPENDIX B

The following tables provide the corresponding numerical values to the tables given in Section 10.

Proton Energy [MeV]	AIM - Integrated Solar Proton Fluence [#/cm2]				
	Transfer	Operation (nominal)	Operation (extended)	Mission Total (nominal)	Mission Total (extended)
1.00E-01	1.48E+12	9.87E+11	7.81E+11	1.95E+12	2.31E+12
2.00E-01	9.40E+11	6.14E+11	4.86E+11	1.26E+12	1.50E+12
5.00E-01	5.17E+11	3.28E+11	2.59E+11	7.06E+11	8.46E+11
1.00E+00	3.29E+11	2.04E+11	1.61E+11	4.56E+11	5.48E+11
2.00E+00	2.09E+11	1.27E+11	1.00E+11	2.94E+11	3.56E+11
2.80E+00	1.68E+11	1.01E+11	7.96E+10	2.38E+11	2.88E+11
4.00E+00	1.26E+11	7.46E+10	5.90E+10	1.82E+11	2.21E+11
5.00E+00	1.05E+11	6.13E+10	4.85E+10	1.53E+11	1.87E+11
6.30E+00	8.40E+10	4.86E+10	3.85E+10	1.24E+11	1.52E+11
8.00E+00	6.58E+10	3.77E+10	2.98E+10	9.81E+10	1.22E+11
1.00E+01	5.18E+10	2.94E+10	2.33E+10	7.81E+10	9.75E+10
1.20E+01	4.16E+10	2.34E+10	1.85E+10	6.32E+10	7.93E+10
1.60E+01	2.91E+10	1.62E+10	1.28E+10	4.48E+10	5.66E+10
2.00E+01	2.15E+10	1.19E+10	9.40E+09	3.34E+10	4.25E+10
2.50E+01	1.55E+10	8.51E+09	6.73E+09	2.43E+10	3.11E+10
2.80E+01	1.30E+10	7.10E+09	5.62E+09	2.04E+10	2.62E+10
3.50E+01	9.02E+09	4.91E+09	3.88E+09	1.43E+10	1.84E+10
4.00E+01	7.17E+09	3.89E+09	3.08E+09	1.14E+10	1.48E+10
5.00E+01	4.77E+09	2.58E+09	2.04E+09	7.65E+09	9.92E+09
6.30E+01	3.03E+09	1.63E+09	1.29E+09	4.88E+09	6.35E+09
8.00E+01	1.84E+09	9.85E+08	7.79E+08	2.98E+09	3.88E+09
1.00E+02	1.11E+09	5.94E+08	4.70E+08	1.81E+09	2.36E+09
1.20E+02	7.35E+08	3.93E+08	3.11E+08	1.19E+09	1.56E+09
1.40E+02	5.11E+08	2.73E+08	2.16E+08	8.31E+08	1.09E+09
1.60E+02	3.70E+08	1.98E+08	1.56E+08	6.01E+08	7.86E+08
2.00E+02	2.12E+08	1.14E+08	8.98E+07	3.45E+08	4.51E+08
2.50E+02	1.19E+08	6.36E+07	5.03E+07	1.93E+08	2.53E+08
3.20E+02	6.02E+07	3.22E+07	2.54E+07	9.78E+07	1.28E+08
4.00E+02	3.25E+07	1.74E+07	1.37E+07	5.28E+07	6.90E+07
5.00E+02	1.75E+07	9.36E+06	7.40E+06	2.85E+07	3.72E+07

Table 1 Solar proton spectrum for selected integral energies for AIM based on a 2020 launch.

Aluminium shielding thickness [mm]	Total ionising radiation dose in Si [rad]				
	Transfer	Operation (nominal)	Operation (extended)	Mission Total (nominal)	Mission Total (extended)
5.00E-02	2.73E+05	1.70E+05	1.34E+05	3.75E+05	4.47E+05
1.00E-01	1.62E+05	9.94E+04	7.86E+04	2.25E+05	2.70E+05
2.00E-01	9.33E+04	5.59E+04	4.42E+04	1.32E+05	1.59E+05
3.00E-01	6.56E+04	3.88E+04	3.07E+04	9.42E+04	1.14E+05
4.00E-01	5.00E+04	2.93E+04	2.31E+04	7.25E+04	8.84E+04
5.00E-01	4.04E+04	2.35E+04	1.86E+04	5.90E+04	7.23E+04
6.00E-01	3.41E+04	1.97E+04	1.56E+04	5.02E+04	6.18E+04
8.00E-01	2.55E+04	1.46E+04	1.16E+04	3.79E+04	4.69E+04
1.00E+00	2.02E+04	1.15E+04	9.11E+03	3.02E+04	3.75E+04
1.50E+00	1.32E+04	7.46E+03	5.90E+03	2.01E+04	2.51E+04
2.00E+00	9.56E+03	5.35E+03	4.23E+03	1.46E+04	1.84E+04
2.50E+00	7.42E+03	4.14E+03	3.27E+03	1.14E+04	1.45E+04
3.00E+00	6.00E+03	3.33E+03	2.64E+03	9.29E+03	1.18E+04
4.00E+00	4.22E+03	2.33E+03	1.84E+03	6.58E+03	8.38E+03
5.00E+00	3.16E+03	1.74E+03	1.37E+03	4.95E+03	6.33E+03
6.00E+00	2.54E+03	1.39E+03	1.10E+03	3.99E+03	5.12E+03
7.00E+00	2.07E+03	1.13E+03	8.95E+02	3.27E+03	4.20E+03
8.00E+00	1.73E+03	9.44E+02	7.47E+02	2.74E+03	3.53E+03
9.00E+00	1.49E+03	8.09E+02	6.40E+02	2.36E+03	3.04E+03
1.00E+01	1.28E+03	6.94E+02	5.49E+02	2.03E+03	2.62E+03
1.20E+01	9.95E+02	5.40E+02	4.27E+02	1.59E+03	2.05E+03
1.40E+01	7.92E+02	4.29E+02	3.39E+02	1.27E+03	1.64E+03
1.60E+01	6.52E+02	3.52E+02	2.79E+02	1.04E+03	1.35E+03
1.80E+01	5.50E+02	2.97E+02	2.35E+02	8.84E+02	1.15E+03
2.00E+01	4.65E+02	2.51E+02	1.98E+02	7.48E+02	9.72E+02

Table 2 TID in silicon for selected spherical shielding thicknesses for AIM based on a 2020 launch.

Aluminium shielding thickness [mm]	Non ionising energy loss equivalent 10 MeV proton fluence [#/cm2]				
	Transfer	Operation (nominal)	Operation (extended)	Mission Total (nominal)	Mission Total (extended)
5.00E-02	5.93E+11	3.69E+11	2.92E+11	8.16E+11	9.77E+11
1.00E-01	3.56E+11	2.19E+11	1.73E+11	4.92E+11	5.87E+11
2.00E-01	1.92E+11	1.15E+11	9.12E+10	2.72E+11	3.28E+11
3.00E-01	1.32E+11	7.80E+10	6.17E+10	1.89E+11	2.30E+11

4.00E-01	1.03E+11	6.01E+10	4.76E+10	1.49E+11	1.82E+11
5.00E-01	8.23E+10	4.79E+10	3.79E+10	1.20E+11	1.48E+11
6.00E-01	6.99E+10	4.04E+10	3.20E+10	1.03E+11	1.27E+11
8.00E-01	5.26E+10	3.01E+10	2.38E+10	7.83E+10	9.69E+10
1.00E+00	4.17E+10	2.37E+10	1.88E+10	6.25E+10	7.77E+10
1.50E+00	2.76E+10	1.56E+10	1.23E+10	4.20E+10	5.27E+10
2.00E+00	2.08E+10	1.16E+10	9.19E+09	3.18E+10	4.01E+10
2.50E+00	1.62E+10	8.99E+09	7.11E+09	2.49E+10	3.16E+10
3.00E+00	1.33E+10	7.36E+09	5.82E+09	2.06E+10	2.61E+10
4.00E+00	9.40E+09	5.18E+09	4.10E+09	1.47E+10	1.87E+10
5.00E+00	7.21E+09	3.96E+09	3.13E+09	1.13E+10	1.45E+10
6.00E+00	5.88E+09	3.22E+09	2.54E+09	9.27E+09	1.19E+10
7.00E+00	4.87E+09	2.66E+09	2.10E+09	7.71E+09	9.92E+09
8.00E+00	4.05E+09	2.21E+09	1.75E+09	6.43E+09	8.29E+09
9.00E+00	3.53E+09	1.92E+09	1.52E+09	5.61E+09	7.24E+09
1.00E+01	3.08E+09	1.67E+09	1.32E+09	4.91E+09	6.34E+09
1.20E+01	2.40E+09	1.30E+09	1.03E+09	3.84E+09	4.96E+09
1.40E+01	1.96E+09	1.06E+09	8.38E+08	3.14E+09	4.07E+09
1.60E+01	1.62E+09	8.72E+08	6.90E+08	2.59E+09	3.37E+09
1.80E+01	1.38E+09	7.42E+08	5.87E+08	2.21E+09	2.88E+09
2.00E+01	1.17E+09	6.30E+08	4.98E+08	1.88E+09	2.45E+09

Table 3 10 MeV equivalent proton fluence for selected shielding thickness for a 2020 launch of AIM.

Aluminium shielding thickness [mm]	**Non ionising energy loss (NIEL) [MeV/g(Si)]**				
	Transfer	Operation (nominal)	Operation (extended)	Mission Total (nominal)	Mission Total (extended)
5.00E-02	5.59E+09	3.48E+09	2.76E+09	7.70E+09	9.21E+09
1.00E-01	3.35E+09	2.06E+09	1.63E+09	4.64E+09	5.53E+09
2.00E-01	1.81E+09	1.09E+09	8.60E+08	2.57E+09	3.09E+09
3.00E-01	1.24E+09	7.36E+08	5.82E+08	1.79E+09	2.17E+09
4.00E-01	9.68E+0	5.67E+08	4.48E+08	1.40E+09	1.71E+09
5.00E-01	7.77E+08	4.52E+08	3.57E+08	1.14E+09	1.39E+09
6.00E-01	6.59E+0	3.81E+08	3.02E+08	9.71E+08	1.20E+09
8.00E-01	4.96E+0	2.84E+08	2.25E+08	7.38E+08	9.14E+08
1.00E+00	3.93E+0	2.24E+08	1.77E+08	5.89E+08	7.33E+08
1.50E+00	2.61E+08	1.47E+08	1.16E+08	3.96E+08	4.97E+08
2.00E+00	1.96E+08	1.10E+08	8.67E+07	3.00E+08	3.78E+08
2.50E+00	1.52E+08	8.48E+07	6.71E+07	2.35E+08	2.98E+08
3.00E+00	1.25E+08	6.94E+07	5.49E+07	1.94E+08	2.46E+08

4.00E+00	8.86E+0	4.88E+07	3.86E+07	1.39E+08	1.77E+08
5.00E+00	6.79E+07	3.73E+07	2.95E+07	1.07E+08	1.37E+08
6.00E+00	5.54E+07	3.03E+07	2.40E+07	8.75E+07	1.12E+08
7.00E+00	4.60E+0	2.51E+07	1.98E+07	7.27E+07	9.35E+07
8.00E+00	3.82E+07	2.08E+07	1.65E+07	6.07E+07	7.82E+07
9.00E+00	3.33E+07	1.81E+07	1.43E+07	5.29E+07	6.83E+07
1.00E+01	2.91E+07	1.58E+07	1.25E+07	4.63E+07	5.98E+07
1.20E+01	2.26E+07	1.23E+07	9.69E+06	3.62E+07	4.68E+07
1.40E+01	1.85E+07	1.00E+07	7.90E+06	2.96E+07	3.84E+07
1.60E+01	1.52E+07	8.23E+06	6.50E+06	2.45E+07	3.17E+07
1.80E+01	1.30E+07	7.00E+06	5.54E+06	2.09E+07	2.71E+07
2.00E+01	1.10E+07	5.94E+06	4.70E+06	1.78E+07	2.31E+07

Table 4 NIEL for selected shielding thickness for AIM based on 2020 launch.

LET [MeV cm²/g]	**Integral Flux [#/m²/sec/sr]**		
	Quiet	Worst Week	Peak 5 Min
1.61E+00	9.46E+07	6.06E+06	3.87E+03
2.30E+00	9.46E+07	6.06E+06	1.17E+03
3.51E+00	9.40E+07	5.99E+06	6.42E+02
8.18E+00	8.25E+07	5.01E+06	2.12E+02
1.24E+01	6.54E+07	3.83E+06	1.11E+02
1.89E+01	4.19E+07	2.38E+06	6.63E+01
2.88E+01	2.14E+07	1.19E+06	4.56E+01
4.35E+01	9.63E+06	5.27E+05	3.57E+01
6.64E+01	3.94E+06	2.14E+05	2.61E+01
1.00E+02	1.57E+06	8.48E+04	1.97E+01
1.50E+02	6.17E+05	3.32E+04	1.14E+01
2.34E+02	1.95E+05	1.05E+04	7.62E+00
3.57E+02	5.62E+04	3.01E+03	4.35E+00
5.39E+02	4.84E+03	2.59E+02	2.83E+00
8.23E+02	1.88E+03	1.09E+02	1.87E+00
1.26E+03	6.16E+02	4.15E+01	8.11E-01
1.90E+03	1.51E+02	1.45E+01	3.23E-01
2.90E+03	8.05E+01	8.02E+00	1.33E-01
4.42E+03	3.99E+01	4.03E+00	5.32E-02
6.68E+03	1.62E+01	1.68E+00	2.10E-02
1.02E+04	6.30E+00	6.62E-01	7.68E-03
1.56E+04	2.19E+00	2.33E-01	2.51E-03
2.35E+04	6.74E-01	7.17E-02	6.84E-04
3.59E+04	1.72E-04	2.56E-05	1.34E-07

5.48E+04	3.07E-05	5.22E-06	4.59E-08
8.37E+04	4.04E-06	7.25E-07	1.01E-08
1.00E+05	8.65E-07	1.56E-07	2.56E-09
1.09E+05	2.03E-09	5.83E-10	2.35E-10
1.61E+00	9.46E+07	6.06E+06	3.87E+03

Table 5 Fluxes for the calculation of SEE/SEU rate as a function of LET.

APPENDIX C

The Didymain shape model is attached to the PDF. Please note that it can be used in the frame of the AIM contracts, however it is still unpublished. The authors (Naidu and Benner) kindly request not to publish the relevant items (such as gravity, slope maps, etc.) and to be co-authors of papers using the data.